

LINEAR VISCOELASTICITY OF CONCENTRATED EMULSIONS

Martin Nemer, Jerzy Blawdziewicz, and Michael Loewenberg
Department of Chemical Engineering, Yale University, New Haven, Conn., USA
michael.loewenberg@yale.edu

Abstract The linear viscoelastic response of an ordered dense emulsion is explored by numerical simulation. At concentrations below maximum packing, the stress relaxation is dominated by a single time scale associated with lubrication, which diverges at maximum packing. For concentrations above maximum packing, the stress relaxation is dominated by fast time scales of the order of the drop relaxation time. A slow time scale appears but does not dominate.

1. INTRODUCTION

The rheology of emulsions and foams is important for a wide range of applications, including polymer processing, personal care products, food processing, textile finishing, and oil recovery. Emulsions have non-Newtonian rheology [1]–[4], including shear thinning and nonzero normal stress differences, and may exhibit a nonzero yield stress. In small-amplitude oscillatory flows, emulsions exhibit a linear viscoelastic response [5].

Experiments and simulations on the low-frequency elastic behavior have focused on the static elastic modulus G_0 , because it is easier to define and measure than the yield stress [6]. The static properties of ordered concentrated emulsions and foams have been investigated theoretically [7]–[9]. In three dimensions the equilibrium behavior of small ordered systems has been studied numerically using minimal-energy simulations [10]. Large systems have been explored in two dimensions using minimal-energy simulations [11], and in three dimensions using simplified effective interparticle potentials to model bubble–bubble interactions [12]–[14].

The dynamical properties of foams and compressed emulsions are less understood. Analytical results for the dynamics of thin inextensible films [15] have been incorporated in theoretical models [16] and simulations [13] of the dynamics of two dimensional systems. In three dimen-

sions, the effective-interparticle-potential model has been supplemented by simple bubble–bubble frictional dissipation [5, 17]. However, these models cannot describe the effect of detailed drop-scale dynamics on the evolution of the system. In general, the development of theories for the rheology of foams and emulsions will require a detailed understanding of the relevant drop-level dynamics.

The focus of this paper is on phenomena that occur on the drop relaxation time scale τ_d . In this paper we explore the linear viscoelastic response of concentrated ordered two-dimensional emulsions and foams in the frequency regime $\omega = O(\tau_d^{-1})$ where the dynamics of drop shape relaxation is important. The response of the system was explored using numerical simulations that incorporate detailed drop-level hydrodynamics.

2. PROBLEM FORMULATION

We consider the linear viscoelastic behavior of a two-dimensional hexagonal array of drops in which both phases are incompressible Newtonian fluids governed by the Stokes equations. Uniform interfacial tension σ_0 is assumed.

At high volume fractions, the drops are in a state of compression. In response, the drop forms flat films and Plateau borders of curvature higher than that of the undeformed drop. In this work we assume that the Plateau borders contain all the continuous phase liquid, and the thin films have zero thickness; thus the hydrodynamics of the thin films simplifies. Details of the boundary conditions at the contact point are discussed in Appendix A.

The magnitude of drop deformation in a flow with shear rate $\dot{\gamma}$ scales with the capillary number $\text{Ca} = \mu a \dot{\gamma} / \sigma_0$, where a is the (volume equivalent) drop radius, and μ is the continuous phase viscosity. The dynamics of the system also depends on the dispersed-to-continuous phase viscosity ratio $\lambda = \hat{\mu} / \mu$, drop volume fraction ϕ , and the external forcing frequency ω . Herein, dimensionless variables are used, where length is scaled with a , time is scaled with drop relaxation time $\tau_d = \mu a / \sigma_0$, and stress is scaled with σ_0 / a .

This work focuses on linear viscoelastic behavior; thus $\text{Ca} \ll 1$. We consider a hexagonal lattice in which the linear relation between stress and strain is isotropic [18]. Accordingly our system is characterized by a single frequency-dependent linear viscoelastic modulus $G(\omega)$.

The drop contribution to the stress, Σ^* , can be expressed in terms of the stress relaxation function Φ :

$$\Sigma^* = \int_{-\infty}^t \Phi(t-t') \dot{\gamma}(t') dt' + \eta_\infty \dot{\gamma}, \quad (1)$$

where $\dot{\gamma}$ is the dimensionless shear rate and η_∞ is the dimensionless effective viscosity of the system in the high-frequency limit. For volume fractions below the critical value ϕ_c (i.e. maximum packing of undeformed drops), the stress relaxation function decays to zero as $t \rightarrow \infty$. At $\phi > \phi_c$ the limiting behavior is $\Phi(t) \rightarrow G_0$. For a two-dimensional hexagonal lattice, the static elastic modulus $G_0 = \frac{1}{2} \sqrt{\phi/\phi_c}$ has been evaluated [8].

In our simulations, the stress relaxation function is obtained by analyzing the response of the system to a step strain. Accordingly the evolution equation is linearized around the equilibrium state \mathbf{x}^* ,

$$\frac{d(\delta\mathbf{x})}{dt} = \mathbf{A} \delta\mathbf{x}, \quad (2)$$

where $\delta\mathbf{x} = \mathbf{x} - \mathbf{x}^*$ is a shape perturbation. In our simulations, the linearized velocity operator \mathbf{A} is obtained by solving the Stokes equations using the boundary-integral method [19]. By projecting the resulting normal modes,

$$\mathbf{A} \mathbf{y}^i = \frac{1}{\tau_i} \mathbf{y}^i, \quad (3)$$

onto a step strain perturbation,

$$\delta\mathbf{x}_s = \sum_i \alpha^i \mathbf{y}^i, \quad (4)$$

the corresponding contribution to the shear stress can be calculated:

$$\Phi(t) = \sum_i \zeta^i e^{-t/\tau_i}. \quad (5)$$

The relation between coefficients α^i and ζ^i is $\zeta^i = \alpha^i s^i$, where s^i is the contribution to the stress from the eigenmode \mathbf{y}^i . The step strain perturbation $\delta\mathbf{x}_s$ is affine with the strain only for $\lambda = 1$; for $\lambda \neq 1$ determining the step strain perturbation requires a calculation of the hydrodynamic field due to the viscosity contrast, in the absence of surface tension. The results presented in the next section have been obtained for $\lambda = 1$.

3. RESULTS

Selected results for the viscoelastic behavior of a monodisperse hexagonal system of drops are presented in Figs. 1–4. Figure 1(a) illustrates

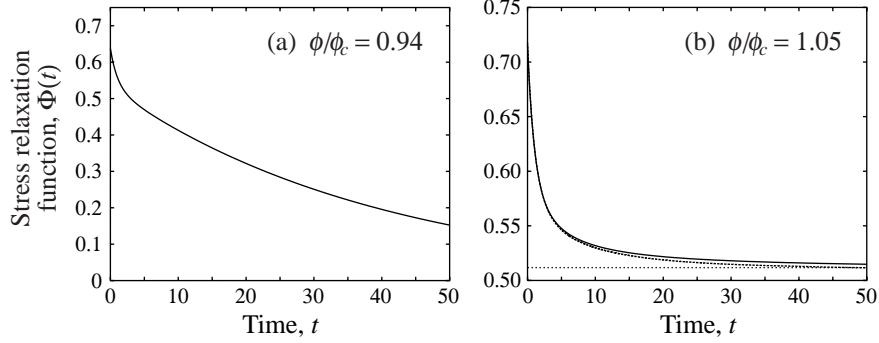


Figure 1 Stress relaxation function nondimensionalized by σ/a , versus time nondimensionalized by drop relaxation time: (a) for $\phi/\phi_c = 0.94$, obtained from the method described in §2 (solid line); (b) for $\phi/\phi_c = 1.05$, obtained from direct step strain simulations—zero-thickness films (solid line), films with finite average thickness $h/a \approx 10^{-3}$ (dashed line), static elastic modulus $G_0(\phi/\phi_c = 1.05)$ (dotted line).

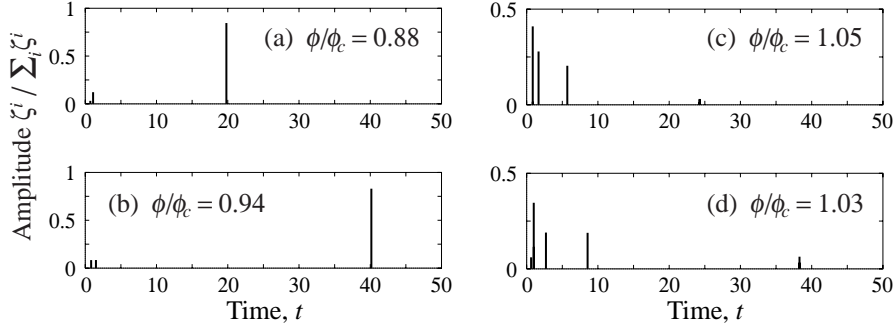


Figure 2 Relaxation spectra as amplitudes ζ^i normalized by $\sum_i \zeta^i$ versus time scaled by drop relaxation time, for $\phi/\phi_c = 0.88, 0.94, 1.05, 1.03$. Volume fractions $\phi/\phi_c = 1.05, 1.03$ were obtained from direct step strain simulations.

the evolution of the stress relaxation function $\Phi(t)$ for dispersed-phase volume fraction below critical, $\phi/\phi_c < 1$, where

$$\phi_c = \frac{\pi}{2\sqrt{3}} \quad (6)$$

for a hexagonal array of cylinders. The results indicate that the stress relaxation function decays to zero at long times. The initial decay occurs on the capillary relaxation time scale τ_d ; however, evolution on a much slower time scale is evident at long times. The relaxation times τ_i and amplitudes ζ^i corresponding to the eigenmode decomposition (5) are plotted in Figs. 2(a,b) for two subcritical values of ϕ . According to our

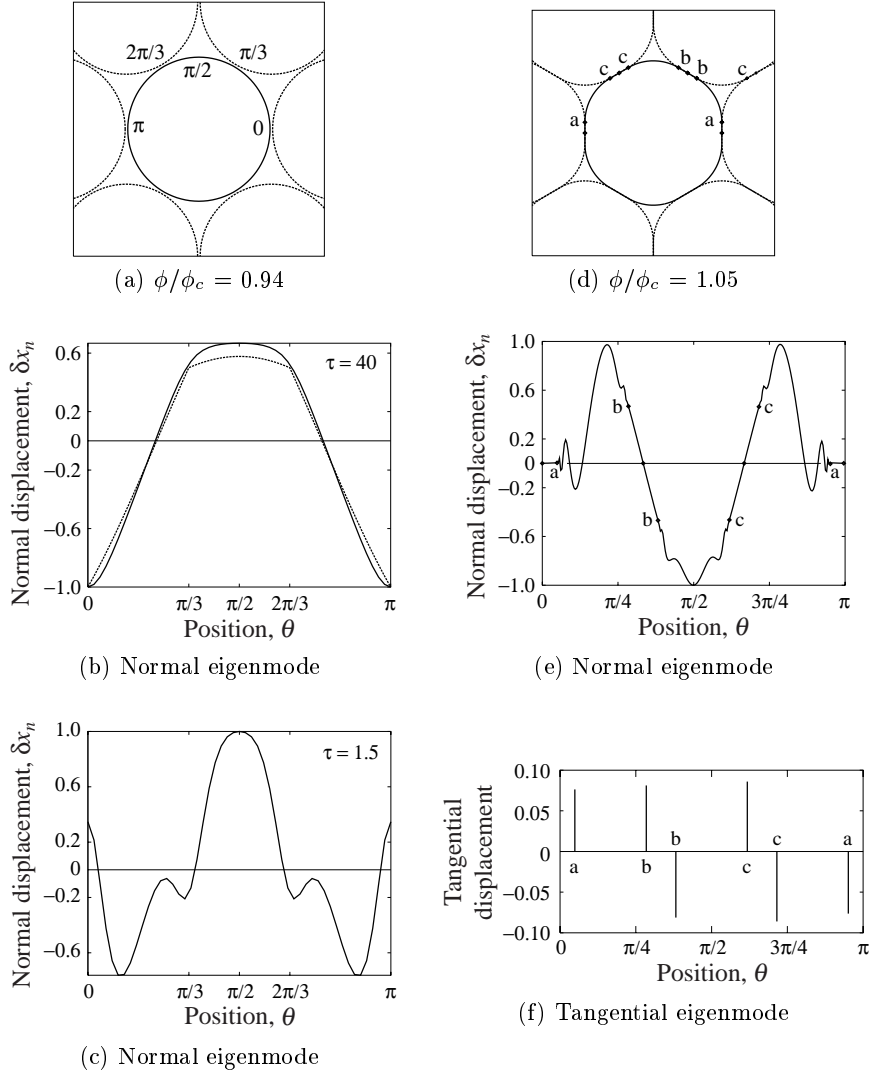


Figure 3 Selected modes for a subcritical and a supercritical volume fraction. (a) Equilibrium drop configuration at $\phi/\phi_c = 0.94$; (b), (c) normal displacements δx_n versus angle defined in (a) (solid lines) for modes with (b) $\tau = 40$ and (c) $\tau = 1.5$. (d) Equilibrium drop configuration at $\phi/\phi_c = 1.05$; (e) normal and (f) tangential displacements for mode with $\tau = 0.8$. Labels a–c in figures (d)–(f) denote contact points. Dashed line in (b) represents analytical result for $\phi/\phi_c \rightarrow 1$.

results, a small number of modes is sufficient to represent $\Phi(t)$ accurately. The dominant mode corresponds to the largest relaxation time associated with the lubrication resistance between closely spaced drops. This slowest time scale diverges as $\phi/\phi_c \rightarrow 1$.

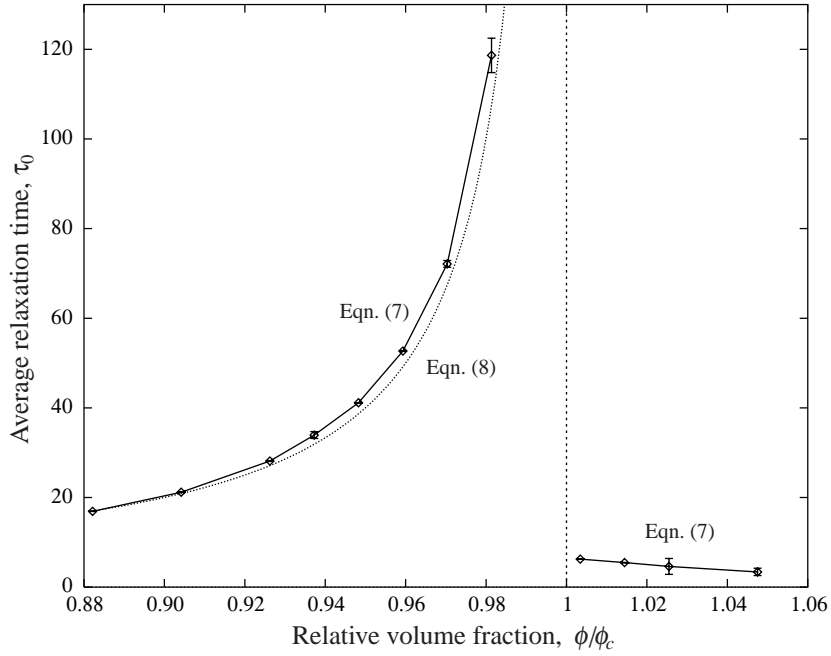


Figure 4 Average time scale τ_0 given by Eqn. (7) versus ϕ/ϕ_c (solid line); average relaxation time from Eqn. (8) (dotted line). Error bars represent the difference between results obtained from zero-thickness film simulations and finite-thickness film simulations. For $\phi/\phi_c = 1.003, 1.014$, results were obtained from simulations with finite-thickness films.

Figure 1(b) shows qualitatively different behavior in the stress relaxation function for $\phi/\phi_c > 1$. At long times, $\Phi(t)$ decays to the static elastic modulus G_0 . In contrast to subcritical volume fractions, the stress relaxation function is dominated by decay on the capillary relaxation time scale τ_d ; a long time scale is evident but with small amplitude. The relaxation times and amplitudes are plotted in Figs. 2(c,d) for two supercritical values of ϕ .

The stress relaxation function obtained from zero-thickness film simulations was compared with the corresponding result for a system with slowly draining films of finite thickness. For average film thickness $h/a \approx 10^{-3}$, the results differ by about 1%, as shown in Fig. 1(b).

Drop-shape perturbations associated with the two slowest modes for a subcritical value of ϕ are shown in Fig. 3(b,c). The slowest mode (solid line plotted in Fig. 3(b)) has the largest amplitude according to Fig. 2(b), and results from the lubrication resistance in the near-contact regions between drops. The dashed line shows the limit as $\phi \rightarrow \phi_c$.

In this limit, drop shape is associated with point forces acting in the lubrication regions of vanishing extent; between the lubrication regions the drop shape is in quasi-static equilibrium due to the separation of the lubrication time scale τ_d/h_0 and the drop relaxation time τ_d , where h_0 is the minimum gap between drops. As the volume fraction decreases, the dominant mode tends continuously to $\cos 2\theta$.

A mode with the relaxation time $\tau_i = O(\tau_d)$ is plotted in Fig. 3(c). In this case, the shape of the drop interface in the Plateau border outside the lubrication regions is significantly perturbed from equilibrium. Oscillations are observed in the near-contact region that corresponds to matching of the time scales for the relaxation inside and outside the lubrication regions.

For $\phi/\phi_c > 1$, the dominant mode (cf. Fig. 2(c)) is shown in Figs. 3(e,f). The central points of the thin films do not move by symmetry, and the films are only weakly deformed in this region. Oscillations observed near contact point a have diminishing amplitude and wavelength. The result shown in Fig. 3(e) indicates that the film a–a increases length, and films b–b and c–c decrease length. These changes in film lengths occur without significant lubrication resistance; thus the mode evolves on drop-relaxation time τ_d .

Figure 4 displays the average relaxation time

$$\tau_0 = \frac{1}{\Phi_0} \int_0^\infty \Phi(t') dt' = \frac{\eta'_0}{\Phi_0}, \quad (7)$$

where η'_0 is the zero-frequency viscosity, and Φ_0 is the drop contribution to the stress immediately after a step strain; for $\lambda = 1$ the initial stress $\Phi_0 = 3/4$. The results indicate that for $\phi < \phi_c$ the average relaxation time diverges as $\phi \rightarrow \phi_c$. This behavior is associated with the lubrication singularity of the zero-frequency viscosity η'_0 at $\phi = \phi_c$. For $\lambda = 1$ Eqns. (7) and (B.8) indicate that

$$\tau_0 = \frac{2}{1 - \phi/\phi_c}, \quad \phi \rightarrow \phi_c. \quad (8)$$

In Fig. 4 this result is represented by the dotted line. The results in Fig. 4 suggest that for $\phi > \phi_c$, τ_0 does not diverge. A more detailed analysis of this phenomenon is underway.

4. CONCLUSIONS

In conclusion, we have performed boundary-integral simulations of the linear viscoelastic response of monodisperse ordered two-dimensional emulsions. Our results indicate that for volume fractions below close

packing of undeformed drops, the evolution is dominated by a single slow mode associated with lubrication resistance. For volume fractions above close packing, the system is dominated by evolution on the drop relaxation time, because thin films between drops can stretch without significant lubrication resistance. There also exists a slow mode that is probably associated with squeezing in the lubrication region where drop interfaces meet, but this mode contributes only weakly to the stress.

As the current work progresses, the effects of system parameters, including volume fraction, viscosity ratio, and contact angle, will be explored. The effects of an insoluble surfactant layer will be also be studied.

Appendix A. Zero-thickness films

In our model the contact point (where three films meet) is convected by the interfacial velocity. A tangential force balance is maintained at the contact point at all times:

$$2\beta\sigma\mathbf{t}_0 = \sigma\mathbf{t}_1 + \sigma\mathbf{t}_2; \quad (\text{A.1})$$

we also assume a continuity relation

$$2\beta\Delta\mathbf{f}_0 = \Delta\mathbf{f}_1 + \Delta\mathbf{f}_2 \quad (\text{A.2})$$

for the normal traction jumps $\Delta\mathbf{f}_i = \kappa\mathbf{n}_i$. Here β is the cosine of the contact angle, κ is the interface curvature, \mathbf{t}_i is the unit tangent vector to interface i , and \mathbf{n}_i is the unit normal vector. The thin film (subscript 0) has two interfaces and is assumed to have negligible thickness compared with the drop size. Subscripts 1 and 2 denote the interfaces of the Plateau border that connect to the thin film.

Appendix B. Low-frequency viscosity for near-critical volume fractions

Here we consider the stress in an ordered emulsion subjected to a linear flow in the limit of low frequency and $\phi \rightarrow \phi_c$ from below. Under these conditions, the drop contribution to the stress is dominated by the lubrication forces at the near-contact regions centered at positions $\mathbf{x}^{(i)}$,

$$\mathbf{F}^{(i)} = R\mathbf{W}^{(i)}, \quad (\text{B.1})$$

where $\mathbf{W}^{(i)}$ is the relative velocity between drops normal to the interface at $\mathbf{x}^{(i)}$ and R is the pairwise lubrication resistance between undeformed drops. Thus,

$$\boldsymbol{\Sigma} = \frac{R}{V_p} \sum_{\text{lattice}} \mathbf{W}^{(i)} \mathbf{x}^{(i)}, \quad (\text{B.2})$$

where V_p is the drop volume,

$$\mathbf{W}^{(i)} = 2a\dot{\gamma} \left(\mathbf{E} : \mathbf{e}^{(i)} \mathbf{e}^{(i)} \right) \mathbf{e}^{(i)}, \quad (\text{B.3})$$

\mathbf{E} is the dimensionless rate-of-strain tensor, $\dot{\gamma}$ is the strain rate, and $\mathbf{e}^{(i)}$ are the lattice vectors.

Combining (B.2) and (B.3) gives

$$\boldsymbol{\Sigma} = \frac{2a^2\dot{\gamma}R}{V_p} \mathbf{A} : \mathbf{E}, \quad (\text{B.4})$$

where

$$A_{ijkl} = \sum_{\text{lattice}} e_i^{(i)} e_j^{(i)} e_k^{(i)} e_l^{(i)} - \frac{1}{m} \delta_{ij} \sum_{\text{lattice}} e_k^{(i)} e_l^{(i)}, \quad (\text{B.5})$$

and m is the dimensionality of the system.

For two-dimensional clean drops in near-contact motion with moderate viscosity ratios $h_0/d \ll \lambda \ll d/h_0$ we find

$$R = 2\pi \frac{\hat{\mu}a}{h_0}, \quad (\text{B.6})$$

where h_0 is the minimum distance between undeformed drops. For a two-dimensional hexagonal lattice,

$$A_{ijkl} = \frac{3}{4} (\delta_{ik} \delta_{jl} + \delta_{il} \delta_{jk} - \delta_{ij} \delta_{kl}). \quad (\text{B.7})$$

Thus, a single transport coefficient

$$\eta'_0 = \frac{3}{2\pi} \frac{\pi \hat{\mu}a}{\delta} \quad (\text{B.8})$$

characterizes the rheology, where $\delta = (1 - \phi/\phi_c)$ is the distance from the critical volume fraction.

References

- [1] Princen, H. M. 1985. Rheology of foams and highly concentrated emulsions: II—Experimental study of the yield stress and wall effects for concentrated oil-in-water emulsions. *Journal of Colloid and Interface Science* **105**, 150–171.
- [2] Princen, H. M., and A. D. Kiss. 1986. Rheology of foams and highly concentrated emulsions: III—Static shear modulus. *Journal of Colloid and Interface Science* **112**, 427–437.
- [3] Princen, H. M., and A. D. Kiss. 1989. Rheology of foams and highly concentrated emulsions: IV—An experimental study of the shear viscosity and yield stress of concentrated emulsions. *Journal of Colloid and Interface Science* **128**, 176–189.

- [4] Mason, T. G., J. Bibette, and D. A. Weitz. 1996. Yielding and flow of monodisperse emulsions. *Journal of Colloid and Interface Science* **179**, 439–448.
- [5] Mason, T. G., M. D. Lacasse, G. S. Grest, D. Levine, J. Bibette, and D. A. Weitz. 1997. Osmotic pressure and viscoelastic shear moduli of concentrated emulsions. *Physical Review E* **56**, 3150–3166.
- [6] Tewari, S., D. Schiemann, D. J. Durian, C. M. Knobler, S. A. Langer, and A. J. Liu. 1999. Statistics of shear-induced rearrangements in a two-dimensional model foam. *Physical Review E* **60**, 4385–4396.
- [7] Princen, H. M. 1979. Highly concentrated emulsions. *Journal of Colloid and Interface Science* **71**, 55–66.
- [8] Princen, H. M. 1983. Rheology of foams and highly concentrated emulsions. *Journal of Colloid and Interface Science* **91**, 160–175.
- [9] Buzzza, D. M. A., and M. E. Cates. 1994. Uniaxial elastic modulus of concentrated emulsions. *Langmuir* **10**, 4503–4508.
- [10] Reinelt, D. A., and A. M. Kraynik. 1996. Simple shearing flow of a dry Kelvin soap foam. *Journal of Fluid Mechanics* **311**, 327–342.
- [11] Weaire, D., T. L. Fu, and Kermode. 1986. On the shear elastic constant of a two-dimensional froth. *Philosophical Magazine B* **54**, L39–L43.
- [12] Lacasse, M. D., G. S. Grest, D. Levine, T. G. Mason, and D. A. Weitz. 1996. Model for the elasticity of compressed emulsions. *Physical Review Letters* **76**, 3448–3451.
- [13] Okuzono, T., and K. Kawasaki. 1993. Rheology of random foams. *Journal of Rheology* **37**, 571–586.
- [14] Durian, D. J. 1995. Foam mechanics at the bubble scale. *Physical Review Letters* **75**, 4780–4783.
- [15] Mysels, K. J., K. Shinoda, and S. Frankel. 1959. *Soap Films: A Study of Their Thinning and a Bibliography*. Tarrytown, N.Y.: Pergamon Press.
- [16] Reinelt, D. A., and A. M. Kraynik. 1990. On the shearing flow of foams and concentrated emulsions. *Journal of Fluid Mechanics* **215**, 1235–1253.
- [17] Durian, D. J. 1997. Bubble-scale model of foam mechanics: Melting, nonlinear behavior, and avalanches. *Physical Review E* **55**, 1739–1751.
- [18] Frisch, U., B. Hasslacher, and Y. Pomeau. 1986. Lattice-gas automata for the Navier–Stokes equation. *Physical Review Letters* **56**, 1505–1508.
- [19] Pozrikidis, C. 1992. *Boundary Integral and Singularity Methods for Linearized Viscous Flow*. Cambridge: Cambridge University Press.